Korean J. Chem. Eng., **25**(4), 905-918 (2008)

Distance transform algorithm for measuring nanofiber diameter

Mohammad Ziabari, Vahid Mottaghitalab, and Akbar Khodaparast Haghi†

University of Guilan, P.O.BOX 3756, Rasht, Iran
(*Received 26 July 2007 • accepted 7 January 2008*)

Abstract−This paper describes a new distance transform method used for measuring fiber diameter in electrospun nanofiber webs. In this algorithm, the effect of intersection is eliminated, which brings more accuracy to the measurement. The method is tested by a series of simulated images with known characteristics as well as some real webs obtained from electrospinning of PVA. Our method is compared with the distance transform method. The results obtained by our method were significantly better than the distance transform, indicating that the new method could successfully be used to measure electrospun fiber diameter.

Key words: Electrospinning, Nanofiber Diameter, Image Analysis, Distance Transform, Novel Technique

INTRODUCTION

Fibers with a diameter of around 100 nm are generally classified as nanofibers. What makes nanofibers of great interest is their extremely small size. Compared to conventional fibers, nanofibers, with higher surface area to volume ratios and smaller pore size, offer an opportunity for use in a wide variety of applications. To date, the most successful method of producing nanofibers is through the process of electrospinning. The electrospinning process uses high voltage to create an electric field between a droplet of polymer solution at the tip of a needle and a collector plate. When the electrostatic force overcomes the surface tension of the drop, a charged, continuous jet of polymer solution is ejected. As the solution moves away from the needle and toward the collector, the solvent evaporates and jet rapidly thins and dries. On the surface of the collector, a nonwoven web of randomly oriented solid nanofibers is deposited [1-8]. Fig. 1 illustrates the electrospinning setup.

The properties of electrospun nanofiber webs depend not only on the nature of the component fibers but also on its structural characteristics. In the last few years, image analysis methods have been developed in order to identify fibers and measure nonwoven characteristics such as fiber orientation [9-16], fiber diameter [17,18], pore size [19], [20], uniformity [21] and other structural features [15,22]. However, since these are new techniques and their accuracy and limitations have not been verified, samples with known characteristics are required to evaluate the accuracy of the methods which can be produced by simulation schemes [9,23].

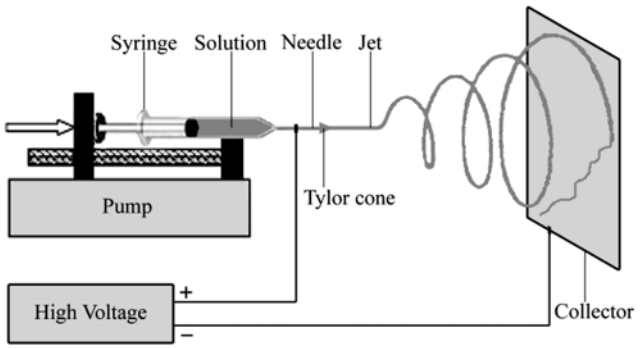

Fig. 1. Electrospinning setup.

†To whom correspondence should be addressed.
E-mail: Haghi@Guilan.ac.ir

Fiber diameter is the most important structural characteristic in electrospun nanofiber webs. Despite the importance, thus far there is no successful method for determining fiber diameter and a few works have been conducted to develop a method for measuring fiber diameter. Furthermore, large scale production of nanofibers requires unique on-line quality control. Hence, developing an accurate and automated fiber diameter measurement technique is useful and crucial. In a method proposed by Pourdyhimi et al. [17], image analysis has been used to measure fiber diameter in nonwoven textiles. Nevertheless, the method has some problems at the intersections of fibers, making it inefficient for measuring electrospun nanofiber diameter. In this contribution, an attempt has been made to circumvent the problems associated with this method, thereby developing a reliable, efficient and automated method for measuring nanofiber diameter in electrospun webs.

METHODOLOGY

1. Fiber Diameter Measurement

Understanding how fiber diameter and its distribution are affected by the electrospinning variables is essential to producing nanofibers with the desired properties. The extremely small fiber size and random production of nanofiber make its diameter measurement very difficult. Most commercially available measurement equipment cannot work with nanofibers [18]. In order to measure fiber diameter, images of the webs are required. These images called micrographs usually are obtained by scanning electron microscopy (SEM), transmission electron microscopy (TEM) or atomic force microscopy (AFM). Dealing with fiber diameter requires high-quality images with appropriate magnifications. The methods for measuring fiber diameter are presented as follows.

1-1. Manual Method

Routine measurement of fiber diameter and its distribution are carried out by manual method using micrographs obtained from

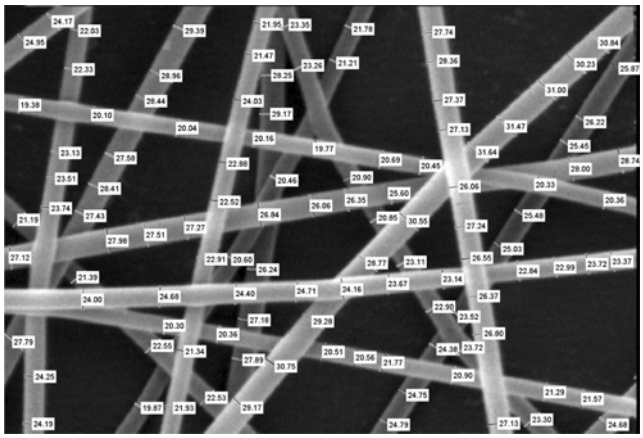

Fig. 2. Manual method.

SEM. First, the length of a pixel in the image is determined, i.e., the scale is set. Then a fiber is selected and pixels between two edges of the fiber perpendicular to the fiber axis are counted. The number of the pixels is then converted to nm by using the scale and the resulting diameter is recorded. This procedure is repeated for other selections until any fiber is processed. Typically, 100 diameters are measured (Fig. 2). Finally, the histogram of fiber diameter distribution is plotted.

This process is very time-consuming and operator consistency and fatigue can reduce the accuracy. Identifying the edges of the fibers requires attention and the measurements are not exactly made perpendicular to the fiber axis. Furthermore, since it is an operator-based method, it cannot be used as on-line method for quality control. Automating the fiber diameter measurement which eliminates the use of an operator is a natural solution to this problem.

1-2. Distance Transform Method

The *skeleton* of an object in a binary image, which provides helpful information about the shape of the object, is defined as the corresponding object with one-pixel width. There are two approaches for assessing the object's skeleton: *skeletonization* and *thinning*. In the first, using medial axis transformation (MAT), the center points of the object which are equidistant form two closest points of the object's boundary are obtained and set to as skeleton [24]. Whereas, in the second, the pixels on the boundary of the object are removed without allowing it to break apart, thereby shrinking a thick object to a centrally located one-pixel width object. In thinning operation, the following conditions must be satisfied:

(1) An object must not break into pieces.

(2) The end points must not be removed so that the object does not become shorter.

(3) An object must not be deleted [25].

Both of these two operations result in line-like structures with one-pixel in thickness preserving the topology of the object. However, the skeleton obtained by skeletonization is often different from that of thinning and has more branches. Fig. 3(a) shows a binary image to which skeletonization and thinning is applied and the resultant skeletons are depicted in Fig. 3(b) and Fig. 3(c), respectively. Note that these operations often produce short *spurs* (also called *parasitic components*) which may further be cleaned up by a post-processing, called *pruning* procedure (Fig. 3(d)). Identifying and removing the spurs iteratively, this procedure is an essential complement to skeletonization and thinning [26].

The distance transform is an operation which is applied to a binary image consisting of 1 s and 0 s corresponding to objects and background, respectively, and results in a grayscale image often called *distance map* (known also as distance transformed image). For each pixel in the binary image, the corresponding pixel in the distance map has the value equal to the minimum distance between that pixel and the closest object pixel, that is, the distance from that pixel to the nearest non-zero valued pixel [25,26]. There are several different sorts of distance transform according to which a distance metric is being used in order to measure the distance between the pixels. Three common distance metrics used in this approach are: city block, chessboard and Euclidean. The city block distance gives the length of a path between the pixels according to a 4-connected neighborhood (moving only in horizontal and vertical directions). The city block distance between (x_1, y_1) and (x_2, y_2) is given by:

$$D_{Cityblock} = |x_1 - x_2| + |y_1 - y_2| \quad (1)$$

In contrast, the chessboard distance metric measures the path between the pixels based on an 8-connected neighborhood (diagonal move is also allowed) as if a King moves in chess. This metric is given by:

$$D_{Chessboard} = \mathrm{Max}(|x_1 - x_2|, |y_1 - y_2|) \quad (2)$$

With the city block metric, distances in the direction of diagonals are longer, resulting in diamond-shaped structures. If a chessboard metric is used, square-shaped structures are obtained [25]. Even though they could be used in certain applications, the Euclidean metric is more practical and relevant, since it is the only one that preserves the isotropy of the continuous space (Fig. 4) [27-29]. The Euclidean distance, which is the straight line distance between two pixels, is defined as:

$$D_{Euclidean} = \sqrt{(x_1 - x_2)^2 + (y_1 - y_2)^2} \quad (3)$$

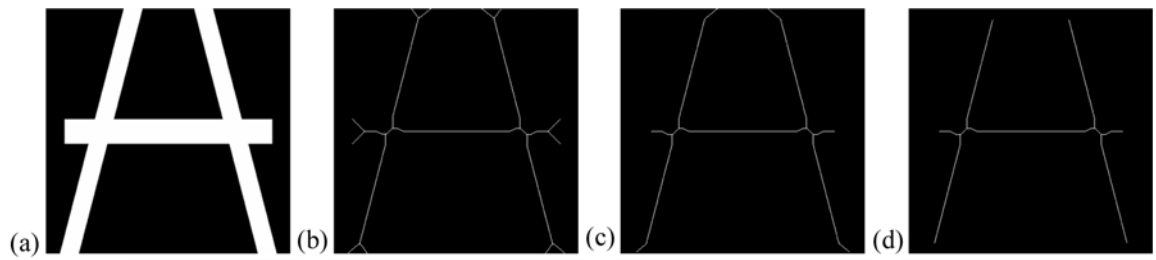

Fig. 3. Obtaining the skeleton of a binary image: (a) a binary image, (b) skeletonization, (c) thinning, (d) resulting skeleton after pruning.

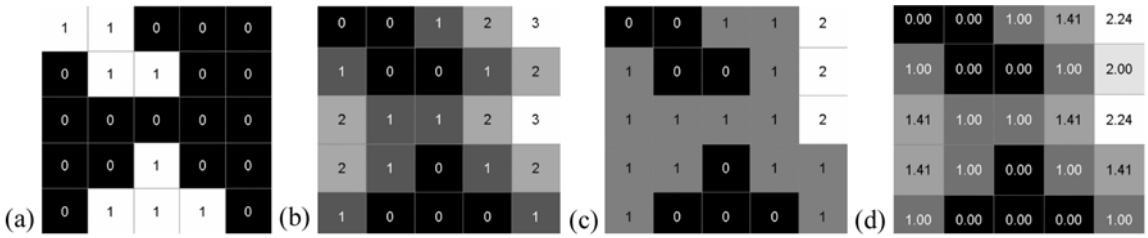

Fig. 4. Distance map of a binary image: (a) a small binary image and its distance map obtained by (b) city block, (c) chessboard, (d) Euclidean metric.

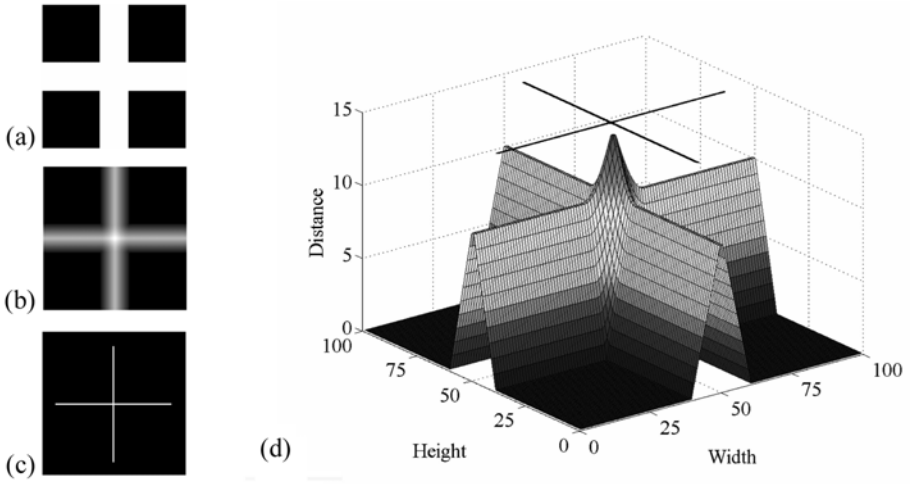

Fig. 5. Skeleton lies exactly over the center of distance map: (a) a simple 100×100 binary image, (b) Euclidean distance map, (c) skeleton obtained by thinning after pruning, (d) 3-D plot showing the coincidence of skeleton and center of the object in distance map.

The center of an object in distance transformed image has the highest value which coincides with the axis of the object. Interestingly, an object's skeleton will lie exactly over the maximum of the distance transform for that object [17]. This fact is clearly demonstrated in Fig. 5. Note that the z-position of the skeleton in Fig. 5(d) is quite arbitrary, just for showing the coincidence. Serving as the basic component of the methods, this remarkable feature will later be utilized for determining nanofiber diameter distribution in electrospun webs.

The algorithm for determining fiber diameter uses the skeleton and distance map of the binary input images. Since our images consist of light fibers on dark background, they first need to be complemented. In the complement of a binary image, zeros become ones and ones become zeros; black and white are reversed [26]. Thus fibers become black and background white. The complemented image is used to create a distance transformed image. Then the skeleton of the objects is created from the input binary image by the process of skeletonization or thinning. Fiber diameter is then determined by using the distance transformed image and the skeleton. The skeleton acts as a guide for tracking the distance map and distances at all points along the skeleton (which coincide with the center of the objects in the distance transformed image) are recorded to compute fiber diameters. Finally, the recorded results are doubled and fiber diameters are obtained. The values (in pixels) may further be converted to nm and the histogram of fiber diameter distribution is plotted. This method was proposed by Pourdeyhimi et al. [17]. Fig. 6 shows a simple simulated image together with its skeleton and distance map including the histogram of fiber diameter obtained by this method.

1-3. New Distance Transform Method

The problem of the distance transform method is that skeletons are often broken at intersection points. Furthermore, since two or more fibers cross each other at the intersections, the value of the center of the object in the distance transformed image doesn't coincide with the fiber diameter because it isn't corresponding to a single fiber. As it is depicted in Fig. 7(a), the intersections in the distance map are brighter than where a single fiber is present. This demonstrates that higher values than expected were returned at these points. Fig. 7(b) shows the broken skeleton at intersections. This problem becomes more pronounced as fibers get thicker and for points where more fibers cross each other. Hence, the distance transform method fails in measuring fiber diameter at intersections.

We modified the distance transform method so that the problems associated with the intersections are solved. Furthermore, in the method proposed by Pourdeyhimi et al. [17], city block distance transform was used which, as mentioned earlier, is not a realistic metric since it does not preserve the isotropy. In order to provide more rational results, in this approach we used the Euclidean distance metric. The method uses a binary image as an input. Then, the distance-transformed image and its skeleton are created. In order to solve the problem of the intersections, these points are identified and deleted from the skeleton.

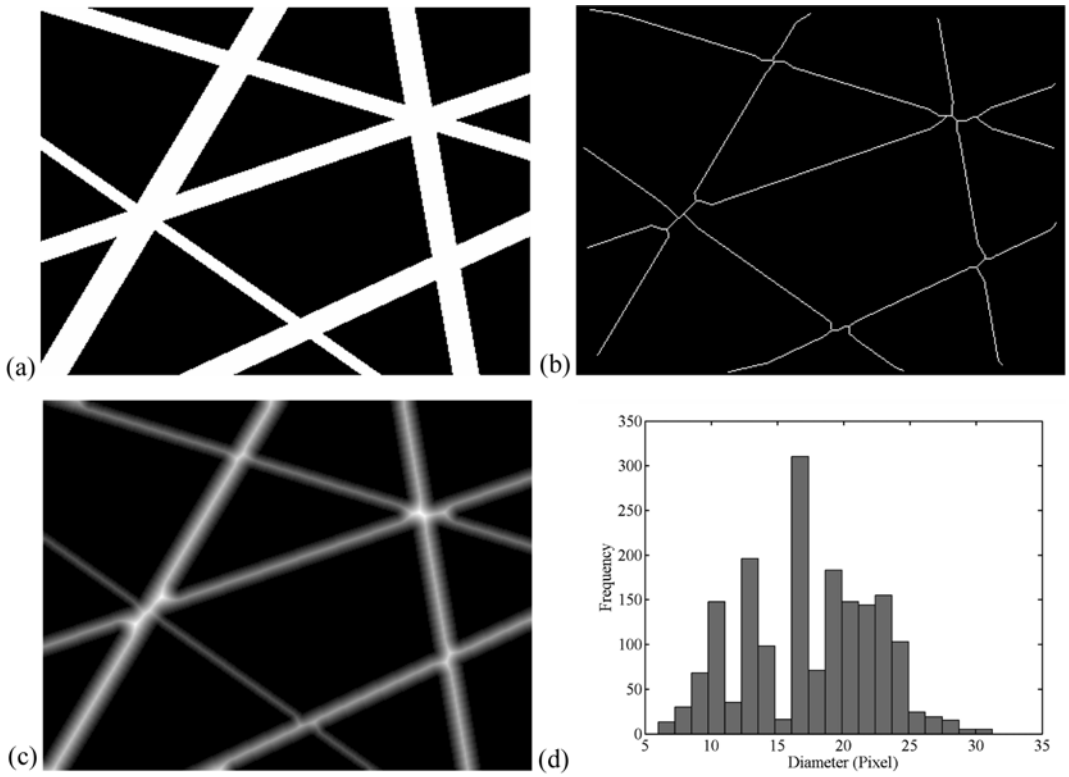

Fig. 6. Distance transform method: (a) a simple simulated image, (b) skeleton of (a), (c) distance map of (a) after pruning, (d) histogram of fiber diameter distribution.

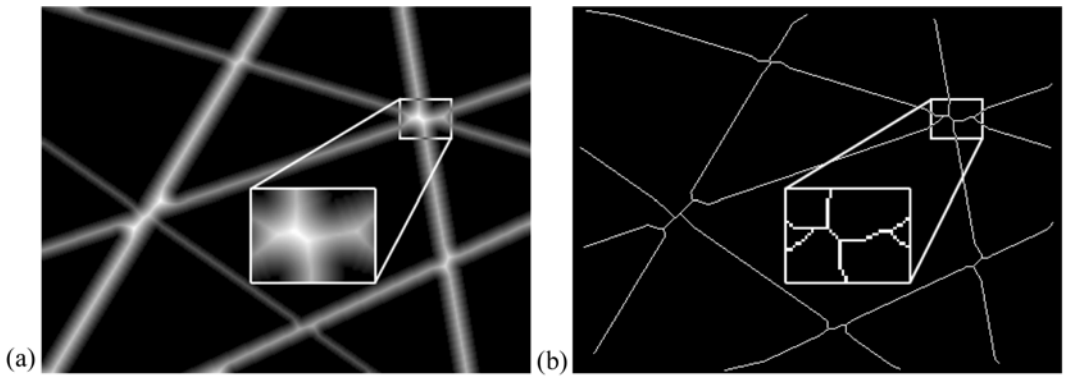

Fig. 7. Distance transform method failure at intersection points: (a) distance map of the image shown in Fig. 6(a), (b) Broken skeleton obtained from thinning of Fig. 6(a) (area around an intersection has been magnified for the sake of clarity).

First, in order to find the intersection points, a *sliding neighborhood operation* is employed. A sliding neighborhood operation is an operation which is applied to a pixel at a time; the value of that pixel in the output image is determined by the implementation of a given function to the values of the corresponding input pixel's neighborhood (Fig. 8). A neighborhood about a pixel, which is usually called the center point, is a square or rectangular region centered at that pixel. The operation consists of five steps:

(1) Defining a center point and a neighborhood block.

(2) Starting from the first (normally top left) pixel in the image.

(3) Performing an operation (a function given) that involves only the pixels in the defined block.

(4) Finding the pixel in the output corresponding to the center pixel in the block and setting the result of the operation as the response at that pixel.

(5) Repeating steps 3 to 4 for each pixel in the input image [26].

Since at an intersection point, two or more fibers meet each other, it could be defined as a location where a white pixel in the skeleton has more than two neighboring pixels each leading a branch. Hence, performing a sliding neighborhood operation on the skeleton with a 3-by-3 sliding block and summation as the function (which is applied over all pixels in the block), the intersections could be identified as the points having values more than 3. This is demonstrated in Fig. 9 (the intersections are shown with arrows).

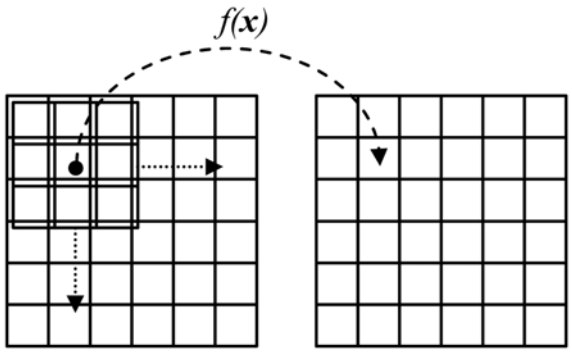

Fig. 8. Sliding neighborhood operation with a 3-by-3 neighborhood block.

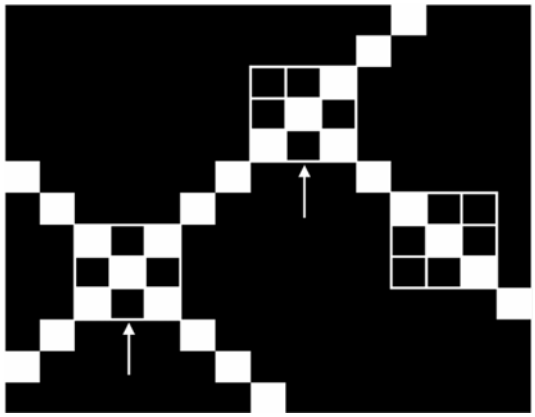

Fig. 9. Identifying intersection points using a sliding neighborhood operation with a 3-by-3 neighborhood block.

After the intersection points are located, the next step is to find the width of each one. This is done by using the distance map of the binary input image via finding the pixel corresponding to that intersection point. The value of the distance map at the pixel is then considered as the width of that intersection. After that, the pixels in the skeleton which lie inside a square with that width around the intersection point are cleaned. This procedure is replicated until each intersection is identified and cleaned. Fig. 10(a) exhibits the skeleton of the simple simulated image shown in Fig. 6(a) after deleting the intersection points followed by a pruning procedure.

Finally, the resultant skeleton (of which the intersections are deleted) is used as a guide for tracking the distance transformed image and fiber diameters are obtained by recording the intensities to at all points along the skeleton (white pixels in Fig. 10(a) show the skeleton) and doubling the results. The distance map of image in Fig. 6(a) is also shown in Fig. 10(b) for better understanding of the procedure. Setting the length of a pixel in the image, the values may then be converted to nm and the histogram of fiber diameter distribution is plotted. Fig. 10(c) demonstrates the histogram of fiber diameter (in term of pixel) obtained by this method. The procedure for determining fiber diameter via this approach is summarized in Fig. 11. The method is efficient, reliable, accurate and very fast and has the capability of being used as an on-line method for quality control.

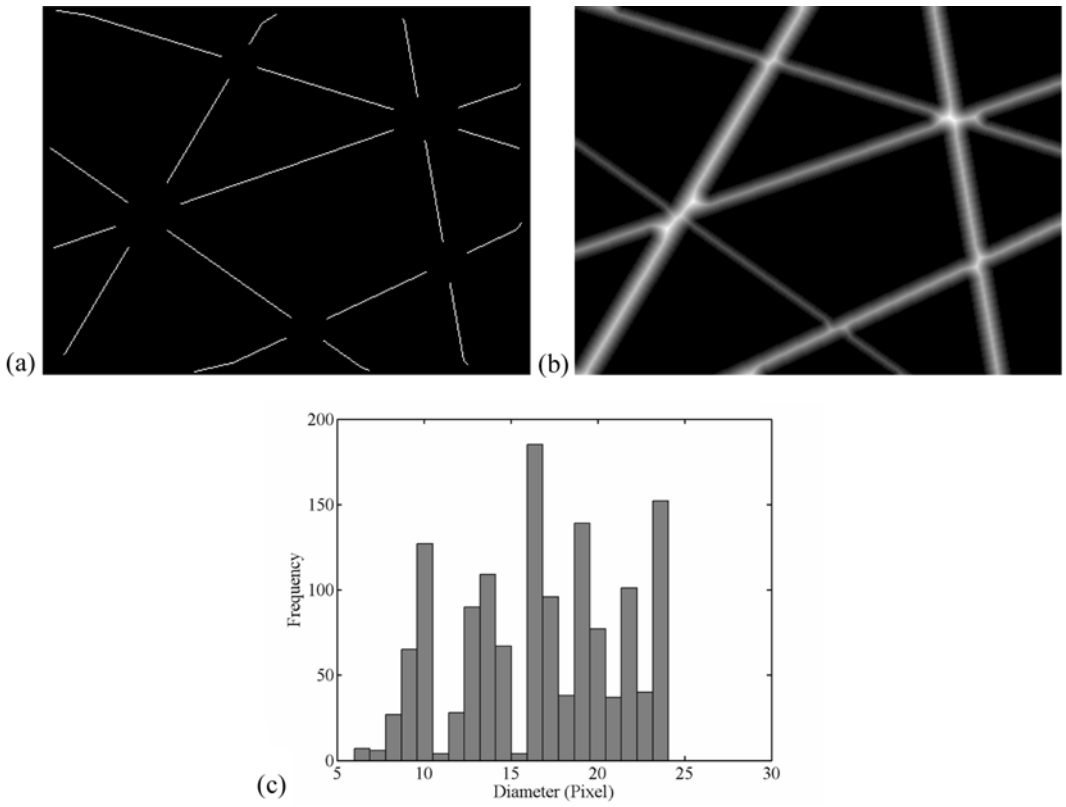

Fig. 10. New distance transform method: (a) the skeleton of the simple simulated image shown in Fig. 6(a) after deleting the intersection points, (b) the distance map, (c) histogram of fiber diameter distribution.

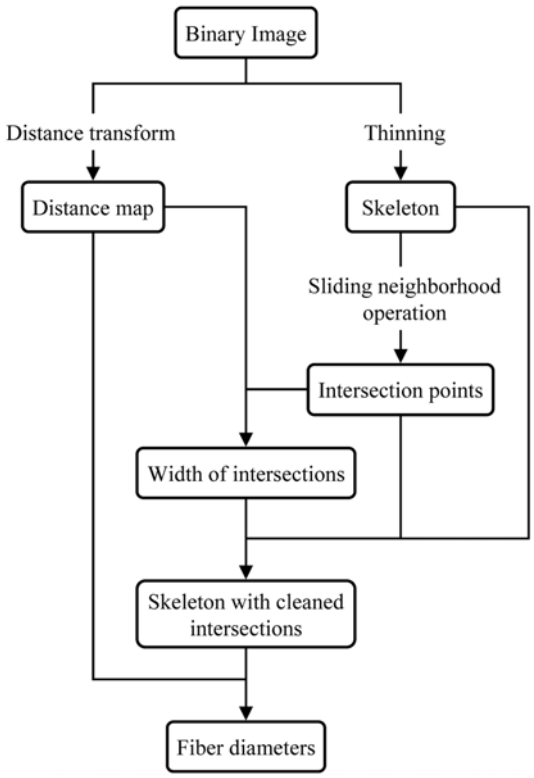

Fig. 11. Flowchart of the new distance transform method.

2. Validation of the Methods

In order to validate the methods for determining fiber diameter, test samples with known characteristics are required. Since it is almost impossible to obtain real electrospun webs with specific characteristics through the experiment and there is not a method which measures fiber diameter precisely to compare the results with, the method will not be well evaluated by merely using real webs. To that end, a simulation algorithm has been employed for generating test samples (which are binary images resemble electrospun webs) with known characteristics. A geometric model has been considered here to simulate electrospun fiberwebs. There are three widely used methods for generating random network of lines. These are called S-randomness, μ-randomness (suitable for generating a web of continuous filaments) and I-randomness (suitable for generating a web of staple fibers). These methods have been described in elaborations by Abdel-Ghani and Davis [23] and Pourdeyhimi et al. [9]. Since the physical characteristics of simulations are known exactly, one can employ them to test the usefulness of the algorithm used in characterizing diameter and other structural features [9]. In this study, μ-randomness procedure has been used for generating simulated images with known characteristics. Under this scheme, a line with a specified thickness is defined by the perpendicular distance d from a fixed reference point O located in the center of the image and the angular position of the perpendicular α. Distance d is limited to the diagonal of the image. Fig. 12 demonstrates this procedure.

One of the most important features of simulation is that it allows several structural characteristics to be taken into consideration with the simulation parameters. These parameters are: web density (controlled as line density), angular density (sampled from a normal or random distribution), distance from the reference point (sampled from a random distribution), line thickness (sampled from a normal distribution) and image size.

3. Thresholding

Fiber diameter determination by the use of image analysis requires the initial segmentation of the micrographs in order to produce binary images. This is a critical step because the segmentation affects the results dramatically. The typical way of producing a binary image from a grayscale image is by *global thresholding* where a single constant threshold is applied to segment the image. All pixels up to and equal to the threshold belong to object and the remaining belong to the background. One simple way to choose the threshold is picking different thresholds until one is found that produces a good result as judged by the observer. Global thresholding, however, is very sensitive to any inhomogeneities in the gray-level distributions of object and background pixels [24-26]. Fig. 13(a) illustrates a typical micrograph obtained from electron microscopy. As it is shown in Fig. 13(b), global thresholding resulted in some broken fiber segments. To eliminate the effect of inhomogeneities, a *local thresholding* scheme could be used. In this approach, the image is divided into subimages where the inhomogeneities are negligible. Then, optimal thresholds are found for each subimage [24-26].

A common practice in this case is to use morphological *opening* to compensate for nonuniform background illumination. The morphological opening is a sequential application of an *erosion* operation followed by a *dilation* operation (i.e., opening=erosion+dilation) using the same *structuring element*. Dilation is an operation that grows or thickens objects in a binary image by adding pixels to the boundaries of objects. Erosion shrinks or thins objects in a binary

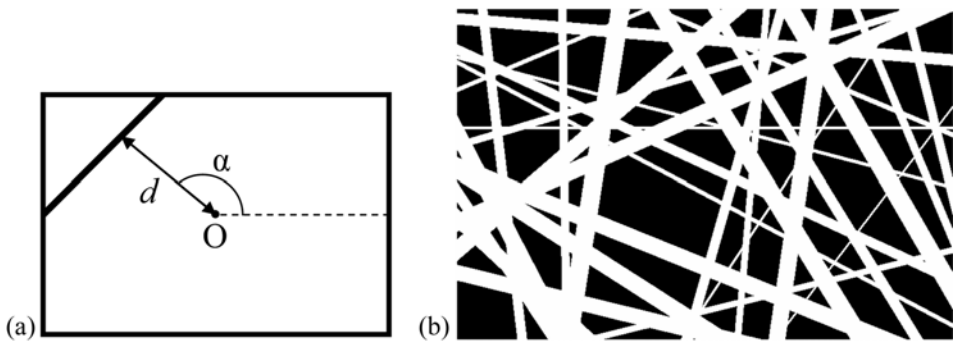

Fig. 12. μ-Randomness: (a) schematic view of the procedure, (b) a typical simulated image generated using this approach.

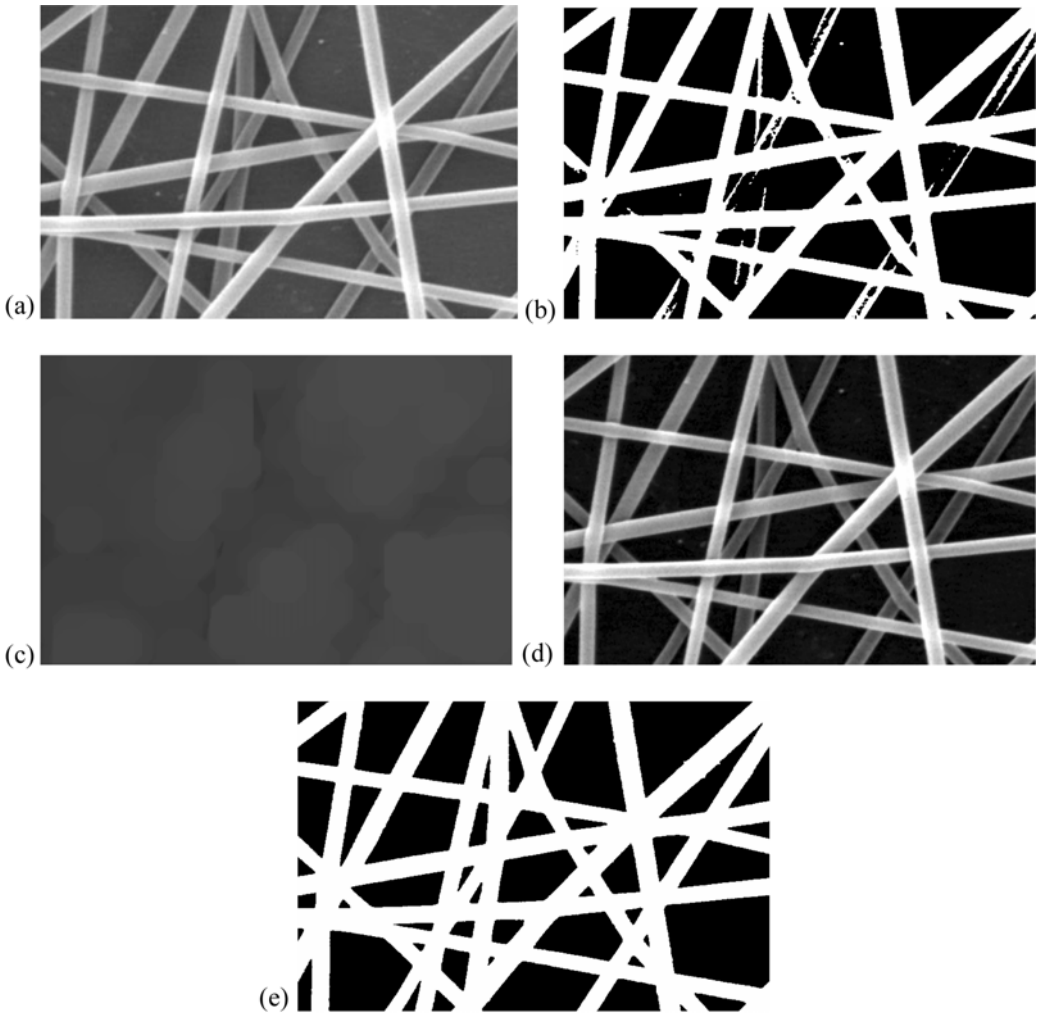

Fig. 13. Thresholding: (a) a typical micrograph of electrospun web, (b) Global thresholding, (c) Opened image, (d) Top-hat transformation, (e) Local thresholding.

image by removing pixels on object boundaries. The specific manner and extent of the thickening or thinning is controlled by the size and shape of the structuring element which is a matrix consisting of 0's and 1's having any arbitrary shape and size. Opening the image produces an estimate of the background provided large enough structuring element is used so that it does not fit entirely within the objects (Fig. 13(c)). Subtracting the opened image from the original image, which is called *top-hat* transformation, results in an image with a reasonably even background (Fig. 13(d)) [24-26]. Now that the background is homogeneous and the edges of the objects are clearer, a global thresholding could be applied to provide the binary image. It could be shown that this process is equivalent to segmenting the image with locally varying thresholds [26].

In order to automatically select the appropriate threshold, *Otsu*'s method [30] is employed. This method is a simple but efficient technique in which the optimal threshold is chosen automatically by the discriminant criterion thereby maximizing the interclass variance and minimizing the intraclass variance of the black and white pixels. Fig. 13(e) depicts the binary image obtained with this approach. As it is apparent, the problem associated with the global thresholding has totally been solved. Note that, since the process is extremely sensitive to noise contained in the image, before the segmentation, a procedure to clean the noise and enhance the contrast of the image is necessary.

EXPERIMENTAL

Electrospun nanofiber webs used as real webs for image analysis were obtained from electrospinning of PVA with average molecular weight of 72,000 g/mol, purchased from MERCK, at different processing parameters. The micrographs of the webs were obtained by using Philips (XL-30) environmental scanning electron microscope (SEM) under magnification of 10,000× after being gold coated. Fig. 14 shows the micrographs of the electrospun webs used as real webs in this study.

RESULTS AND DISCUSSION

We have evaluated the accuracy of the fiber diameter determined by the two methods using two sets of test samples each composed of five simulated images. The first set images had constant diameters which increased from 5 to 25 pixels for different samples. The

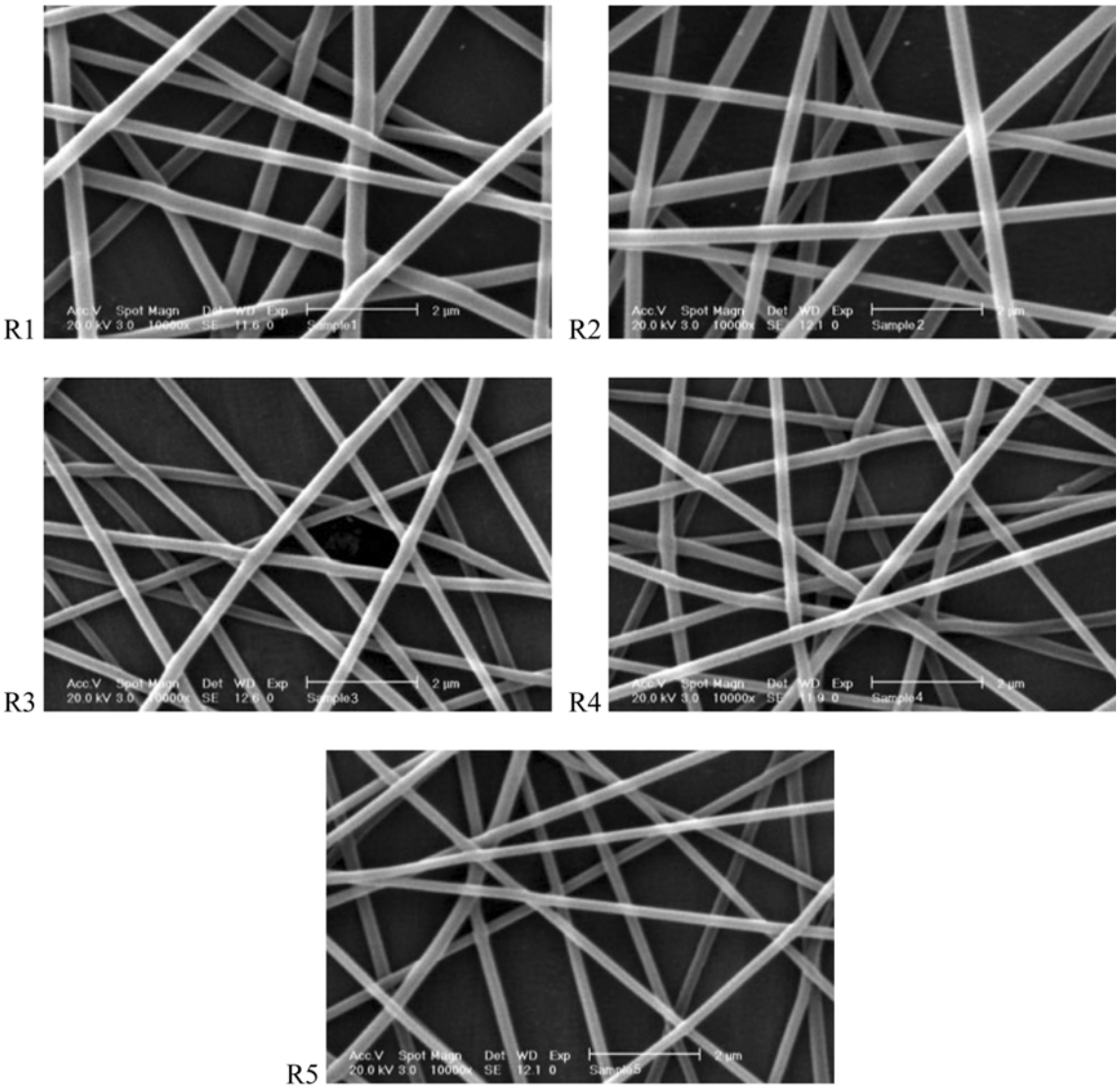

Fig. 14. Micrographs of the electrospun webs.

Table 1. Structural characteristics of first set images

Image no.	Angular range	Line density	Line thickness
C1	0-360	30	5
C2	0-360	30	10
C3	0-360	30	15
C4	0-360	30	20
C5	0-360	30	25

Table 2. Structural characteristics of second set images

Image no.	Angular range	Line density	Line thickness	
			Mean	Std
V1	0-360	30	15	2
V2	0-360	30	15	4
V3	0-360	30	15	6
V4	0-360	30	15	8
V5	0-360	30	15	10

second set images had varying diameter sampled from normal distributions with a mean of 15 pixels and standard deviation of 2 to 10 pixels. For both cases the line density was set to 30 and the angular density sampled from a random distribution in the range of 0-360°. The simulation parameters for the two sets are presented in Table 1 and Table 2. Fig. 15 and Fig. 16 show the simulated images in the two sets.

The results for the simulated images are given in Table 3 and Table 4. Fig. 17 and Fig. 18 show the distribution of fiber diameter for the two sets of simulated images obtained by the methods. A normal distribution was also fitted on the histogram in each case.

From Table 3 and Table 4 it is apparent that for all the simulated samples, the results obtained by the new method were significantly better than the old one. For both sets of simulated images, the mean and standard deviation of fiber diameter obtained by new distance transform were very close to those of simulation. It is noteworthy that the true mean and standard deviation of diameter in samples

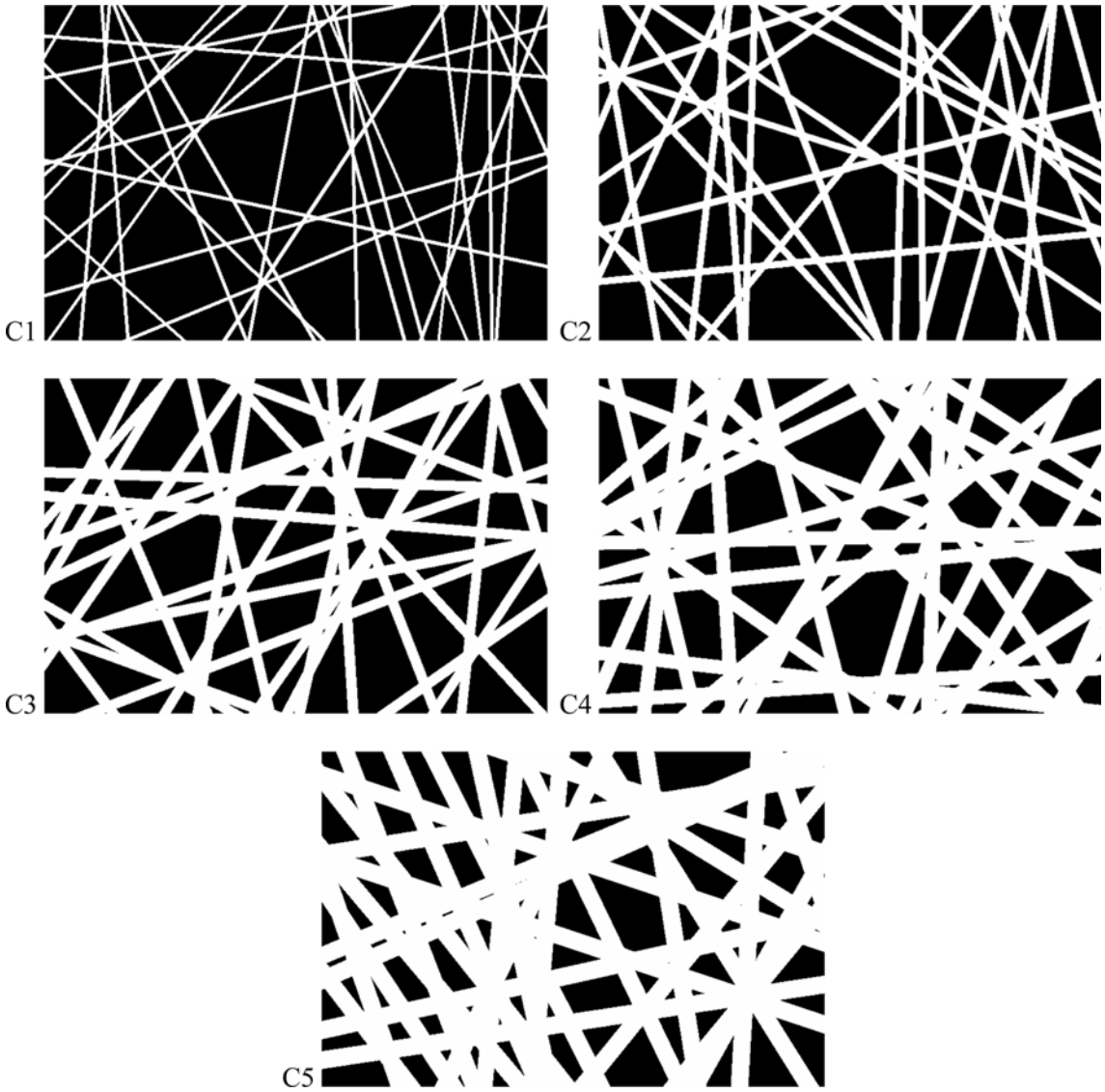

Fig. 15. Simulated images with constant diameter.

with varying line thickness slightly differ from those used as simulation parameters (see Table 2).

As described earlier, the distance transform method fails in measuring the fiber diameter at intersection points. The intersections cause an overestimation of fiber diameter. Since in our developed method these points were deleted, the effects of intersections which cause imprecise measurement of fiber diameter were eliminated. Therefore, the fiber diameter was determined more accurately.

Both methods do not distinguish multiple fibers being joined together. This can happen in simulation by laying one line over the other. In real webs, fiber bundling sometimes happens (often in high density webs which consist of many fibers). Since there is not any black pixel (associated with the background) between joined fibers, they are segmented as a single fiber in the step of thresholding.

There may also be up to half a pixel error in both directions, which turns out to be up to 1 pixel error in measuring fiber diameter. The error may be more significant when the fibers are thicker.

The slight difference between the diameters obtained by our method and simulation can be attributed to the 1-pixel measurement error, bundling of fibers, remaining some parts of branches after pruning and slight variations of skeleton adjacent to intersections which weren't deleted. The last two problems could easily be solved by further pruning for the former and increasing the area to be deleted for each intersection for the later. But because it causes a decrease in the number of diameter measurements, the authors preferred to leave it in this manner. It can be shown that the errors due to these problems do not play an important role in variation of the diameter since they are in the range of measurement error. Furthermore, some parts of the image due to the presence of intersections are deleted and not counted in diameter measurement; this can be another reason for the variation observed. In most cases except where thick fibers are present, the difference between our method and simulation was within the 1-pixel measurement error. That is, the effects of other errors are negligible.

In addition there were five real webs in this study for testing the applicability of the methods for real samples. The results for the

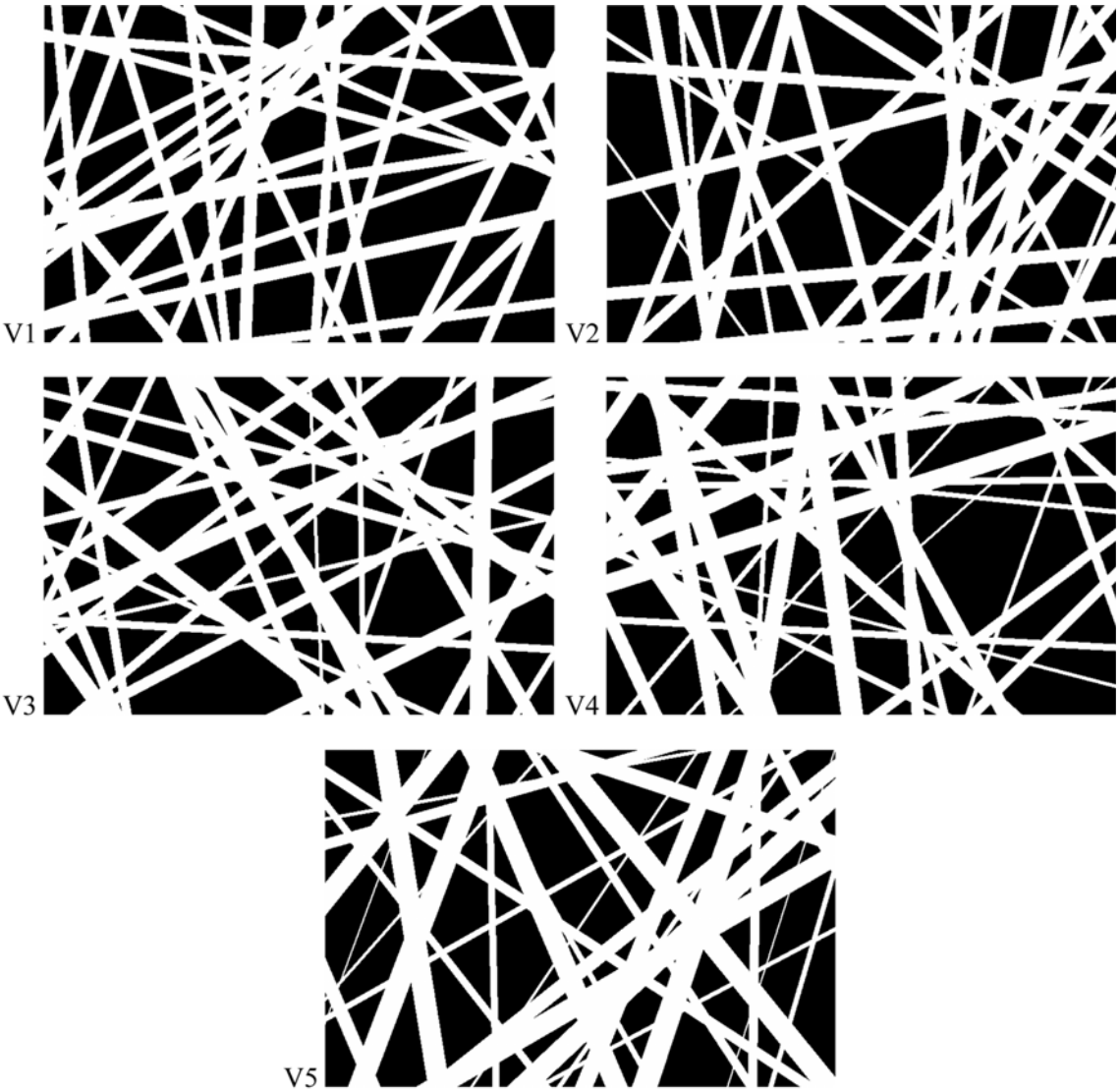

Fig. 16. Simulated images with varying diameter.

Table 3. Mean and standard deviation for series 1

		C1	C2	C3	C4	C5
Simulation	mean	5	10	15	20	25
	std	0	0	0	0	0
Distance transform	mean	5.486	10.450	16.573	23.016	30.063
	std	1.089	2.300	5.137	6.913	10.205
New distance transform	mean	5.366	9.917	15.106	20.013	24.645
	std	0.747	1.053	1.707	1.765	2.837

Table 4. Mean and standard deviation for series 2

		V1	V2	V3	V4	V5
Simulation	mean	15.247	15.350	15.243	15.367	16.628
	std	1.998	4.466	5.766	8.129	9.799
Distance transform	mean	16.517	16.593	17.135	17.865	19.394
	std	5.350	6.165	7.597	9.553	11.961
New distance transform	mean	14.876	15.020	14.812	14.651	15.546
	std	2.403	4.797	6.047	7.851	9.942

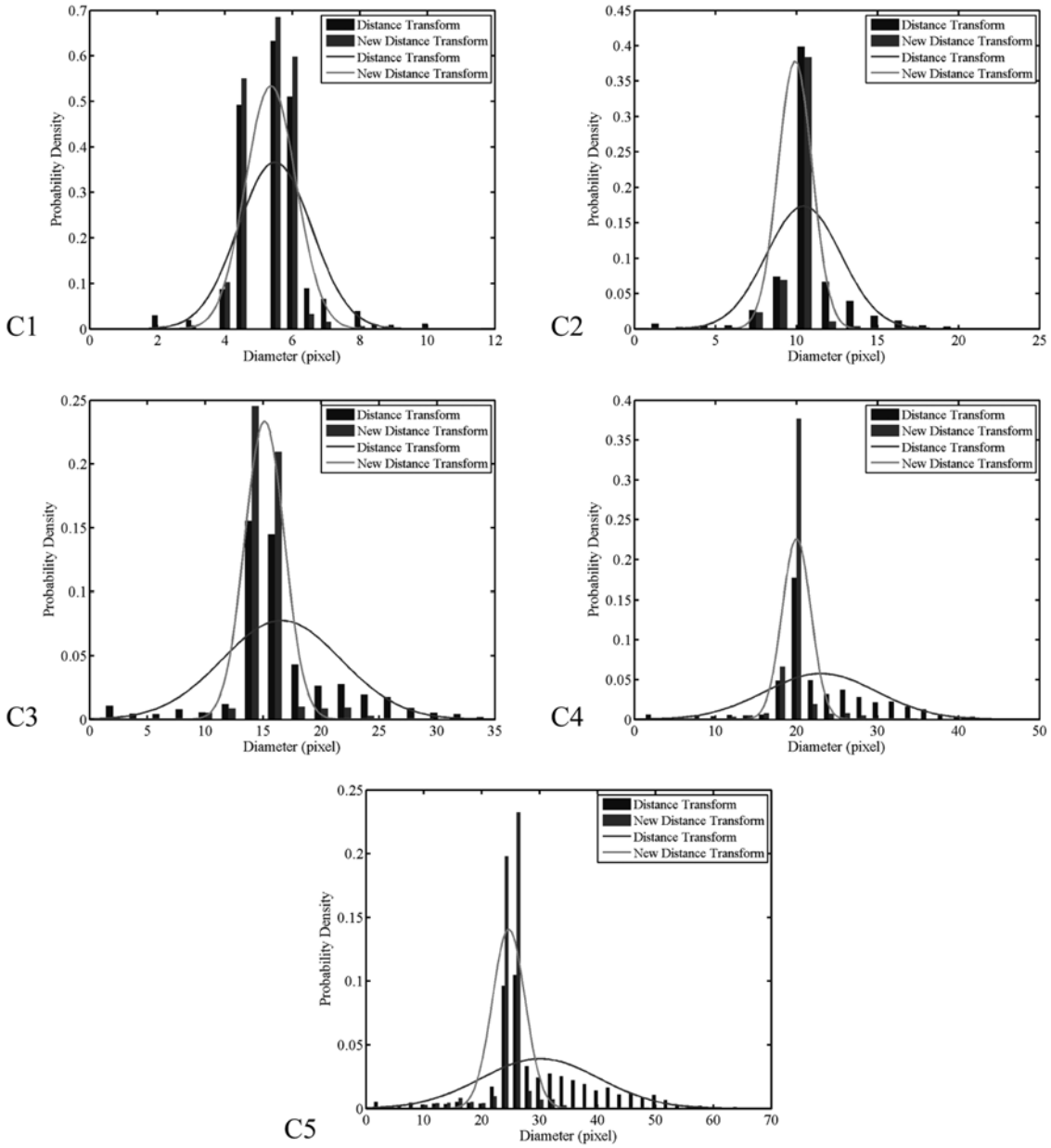

Fig. 17. Histograms for simulated images with constant diameter.

real webs obtained by two methods together with manual method are presented in Table 5. Fig. 19 shows the diameter distribution of these samples in terms of nm. The curved line over each histogram corresponds to its fitted normal distribution.

The results for the real webs are in complete agreement with the trends observed by the simulation. Mean and standard deviation of fiber diameter obtained by our method are very close to those obtained by manual method. In addition to the above mentioned reasons, the differences here can also be attributed to a different number of measurements. For each sample, our method measured over 2,000 fiber diameters, whereas the operator could only measure 100 fiber diameters (in manual method) because of the time-consuming nature of this work. Despite all of these facts, the differences here are also within the 1-pixel measurement error, which suggests that other errors are less significant.

CONCLUSION

Fiber diameter is an important structural characteristic in electrospun webs. Understanding how it is affected by processing variables is essential for producing nanofibers with desired properties. Electrospun fiber diameter is often measured by manual method, which is a time-consuming operator-based technique that cannot be used for on-line quality control. An image analysis based method called distance transform was reported in the literature as an automated technique for fiber diameter measurement in nonwoven textiles. Despite the usefulness, the method fails in measuring the diameter at intersections since both the skeleton and distance map are broken at these points, thereby the center of the object in a distance transformed image no longer coincides with the fiber diameter. We developed a novel method in which the intersections are identified

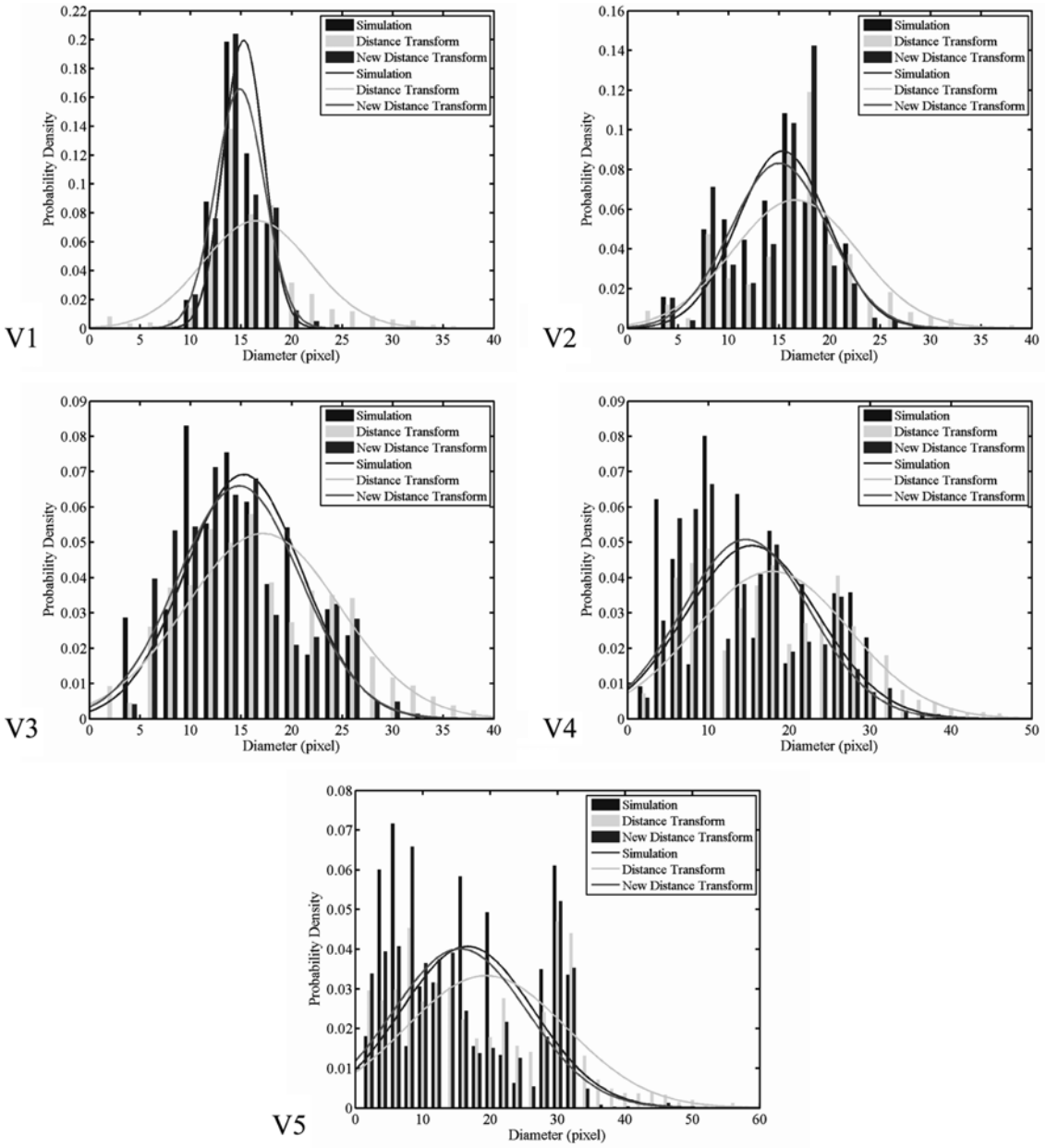

Fig. 18. Histograms for simulated images with varying diameter.

Table 5. Mean and standard deviation for real webs

			R1	R2	R3	R4	R5
Manual	mean	pixel	24.358	24.633	18.583	18.827	17.437
		nm	318.67	322.27	243.11	246.31	228.12
	std	pixel	3.193	3.179	2.163	1.984	2.230
		nm	41.77	41.59	28.30	25.96	29.18
Distance transform	mean	pixel	27.250	27.870	20.028	23.079	20.345
		nm	356.49	364.61	262.01	301.94	266.17
	std	pixel	8.125	7.462	4.906	7.005	6.207
		nm	106.30	97.62	64.18	91.64	81.21
New distance transform	mean	pixel	24.741	25.512	18.621	20.100	18.299
		nm	323.681	333.767	243.610	262.954	239.395
	std	pixel	3.854	3.961	2.826	2.903	2.795
		nm	50.417	51.821	36.976	37.980	36.571

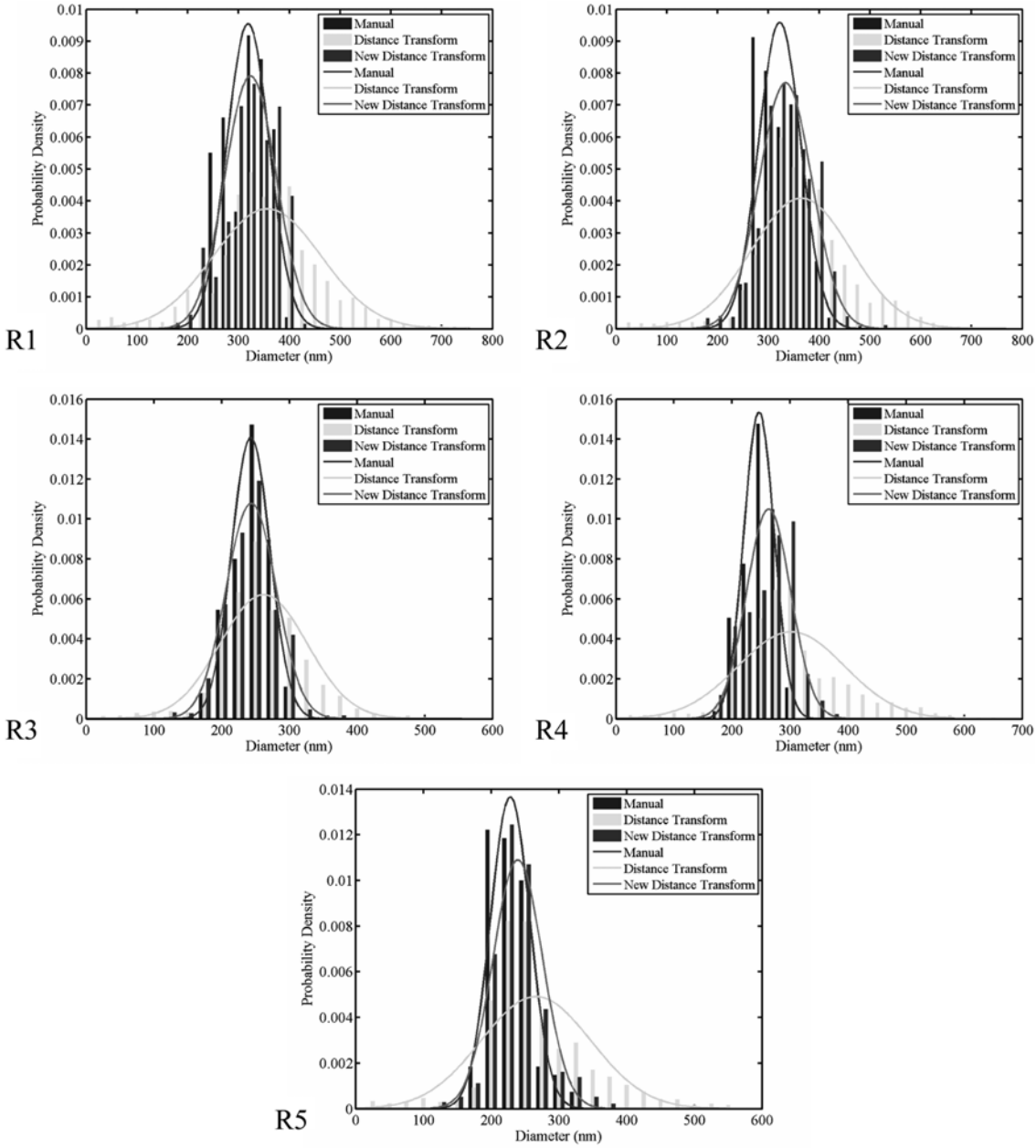

Fig. 19. Histograms for real webs.

and deleted from the skeleton, thus solving the associated problem. The techniques have been validated by applying the methods to test images with known characteristics generated by using μ-randomness procedure. The results show the effectiveness of our method for diameter measurement. For the entire simulated images the new algorithm resulted in mean and standard deviation of fiber diameter closer to the simulation. In addition, five electrospun webs of PVA were used in order to test the general applicability of the methods for real webs. Due to the need of binary input image, local thresholding was applied to the micrographs of the webs obtained from SEM. Otsu's method was used in order to automatically determine the appropriate threshold. The results for the real webs show that mean and standard deviation of fiber diameter obtained by new algorithm were in perfect agreement with the manual method. That is, our attempt to develop a method for measuring fiber diameter has been quite successful.

ACKNOWLEDGMENT

The authors would like to gratefully acknowledge the reviewers who have donated the hours necessary to review this article. We thank you for their helpful and important comments on this manuscript.

REFERENCES

1. A. K. Haghi and M. Akbari, *Phys. Stat. Sol. (a)*, **204**, 1830 (2007).
2. J. Doshi and D. H. Reneker, *J. Electrostatics*, **35**, 151 (1995).

3. H. Fong and D. H. Reneker, *Electrospinning and the formation of nanofibers*, In: D. R. Salem, *Structure formation in polymeric fibers*, Hanser, Cincinnati (2001).
4. D. Li and Y. Xia, *Advanced Materials*, **16**, 1151 (2004).
5. Z.-M. Huang, Y.-Z. Zhang, M. Kotaki and S. Ramakrishna, *Compos. Sci. Technol.*, **63**, 2223 (2003).
6. H. S. Park and Y. O. Park, *Korean J. Chem. Eng.*, **22**, 165 (2005).
7. G. T. Kim, Y. J. Hwang, Y. C. Ahn, H. S. Shin, J. K. Lee and C. M. Sung, *Korean J. Chem. Eng.*, **22**, 147 (2005).
8. G. T. Kim, J. S. Lee, J. H. Shin, Y. C. Ahn, Y. J. Hwang, H. S. Shin, J. K. Lee and C. M. Sung, *Korean J. Chem. Eng.*, **22**, 783 (2005).
9. B. Pourdeyhimi, R. Ramanathan and R. Dent, *Text. Res. J.*, **66**, 713 (1996).
10. B. Pourdeyhimi, R. Ramanathan and R. Dent, *Text. Res. J.*, **66**, 747 (1996).
11. B. Pourdeyhimi, R. Dent and H. Davis, *Text. Res. J.*, **67**, 143 (1997).
12. B. Pourdeyhimi and R. Dent, *Text. Res. J.*, **67**, 181 (1997).
13. B. Pourdeyhimi, R. Dent, A. Jerbi, S. Tanaka and A. Deshpande, *Text. Res. J.*, **69**, 185 (1999).
14. B. Pourdeyhimi and H. S. Kim, *Text. Res. J.*, **72**, 803 (2002).
15. B. Xu and Y. L. Ting, *Text. Res. J.*, **65**, 41 (1995).
16. I. Krucinska and S. Krucinski, *Text. Res. J.*, **69**, 363 (1999).
17. B. Pourdeyhimi and R. Dent, *Text. Res. J.*, **69**, 233 (1999).
18. D. M. Luzhansky, *Quality control in manufacturing electrospun nanofiber composites*, International nonwovens technical conference, Baltimore, Maryland (September 15-18, 2003).
19. H. S. Kim and B. Pourdeyhimi, *Intern. Nonwoven J.*, 15-19 (Winter 2000).
20. A. H. Aydilek, S. H. Oguz and T. B. Edil, *J. Comput. Civil Eng.*, 280-290 (2002).
21. R. Chhabra, *Intern. Nonwoven J.*, 43-50 (Spring 2003).
22. E. Ghassemieh, H. K. Versteeg and M. Acar, *Intern. Nonwoven J.*, 26-31 (Summer 2001).
23. M. S. Abdel-Ghani and G. A. Davis, *Chem. Eng. Sci.*, **40**, 117 (1985).
24. W. K. Pratt, *Digital image processing*, 3rd Ed., John Wiley and Sons, New York (2001).
25. B. Jähne, *Digital image processing*, 5th Ed., Springer, Germany (2002).
26. R. C. Gonzalez and R. E. Woods, *Digital image processing*, 2nd Ed., Prentice Hall, New Jersey (2001).
27. H. Breu, J. Gil, D. Kirkpatrick and M. Werman, *IEEE T. Pattern Anal.*, **17**, 529 (1995).
28. N. Sudha, S. Nandi, P. K. Bora and K. Sridharan, *Efficient computation of euclidean distance transform for applications in image processing*, Proceedings of IEEE Region 10 International Conference on Global Connectivity in Energy, Computer, Communication and Control, 49-52 (1998).
29. Q.-Z, Ye, *The signed euclidean distance transform and its applications*, Proceedings of the 9th International Conference on Pattern Recognition, Rome, Italy, 495-499 (1988).
30. N. Otsu, *IEEE T. Syst. Man. Cy.*, **9**, 62 (1979).